



OPEN Identification method of wheel-rail two-point contact state in switch area

Ping Lu¹, Xinyi Li², Dabin Cui²✉, Boyang An³ & Wenpeng Jiang²

Two-point contact is one of the fundamental problems of wheel-rail contact in switch area. The contact state and the distribution of forces are complex and essential points in wheel-rail relationship. Given the problem that the current dynamic wheel-rail contact state is challenging to detect, a theory to detect the two-point contact state of the wheel-rail in switch area using a discrete gauge column was presented and proved in the finite element model. This paper derived the relationship between strain gauge position and stress using a modified rail model. The patch scheme was determined using the rail waist bending moment difference method to achieve decoupling of the bridge circuit of the force measurement columns. The bridge circuit was calibrated by means of the modified theoretical calibration method, and the circuit test data was obtained for the two-point contact condition in the switch area. The study compared the results obtained from the wheel-rail column finite model and circuit test data for two-point contact conditions, demonstrated the method's ability to identify the two-point contact state and the wheel-rail force distribution characteristics in the switch area. The results show that the method can identify the two-point contact state in switch area and distribute characteristics of the wheel-rail force. And the wheel-rail contact point position can be deduced accurately according to the wheel-rail force. This test method provides a test verification scheme for wheel-rail two-point rolling contact theory and a new technology for the dynamic force testing of wheel-rail in switch area.

Keywords Two-point contact, Force-measuring switch, Contact force, Contact status identification

The location of wheel-rail contact points and load distribution within the contact patch are essential parameters for evaluating the wheel-rail matching state. Some advanced theories are proposed through extensive research in this field, which are widely used in the case of single-point contact^{1–3}. Still, in the case of two-point contact in switch area, obtaining the accurate wheel-rail contact state by theoretical calculation is difficult because the instantaneous center of velocity and load distribution at the two contact points cannot be determined.

The test method is another important way to study the wheel-rail contact characteristics, among which the strain gauge method is one of the most commonly used wheel-rail force test methods. The strain gauge method usually arranges the strain gauge on the particular position of the vehicle or rail to make the special force measuring equipment. In these force-measuring equipment, the strain gauge is usually arranged on the axle⁴, wheel web⁵, primary suspension⁶ and rail web⁷, etc. The dynamometric wheelset⁸ is a typical wheel-rail force measuring device employing strain gauges that are commonly used in the industry. Hiromichi Kanehara et al.⁹ introduced the application of a strain gauge in the measurement of wheel-rail contact point position and pointed out that the lateral distribution of compress strain caused by the vertical load in that area can measure the position of the contact point without the effect of bend caused by lateral force. Because the elastic deformation of the wheel is more sensitive to the vertical force of the wheel and rail, the dynamometric wheel has high measurement accuracy. However, due to the small wheel-rail contact patch, the difference in the position of the contact points on the wheel-rail interface cannot be reflected in the strain of the wheel web, which leads to difficulty in identifying the position of the contact points.

Zhou et al.⁷ derived a strain gauge configuration based on the vertical strain sum. Peng et al.⁸ employed the shear method to quantify the wheel-rail force, and their findings indicated that wheel-rail impact resulting from wheel flattening exerts a notable influence on the wheel/guideway force. Lan et al.¹⁰ developed a bidirectional gated recurrent unit (GRU) that inverts the time history curve of wheel-rail forces. Ropalkar and his colleagues¹¹

¹Sichuan Provincial Engineering Research Center of Rail Transit Lines Smart Operation and Maintenance, Chengdu Vocational & Technical College of Industry, Chengdu 610218, China. ²School of Mechanical Engineering, Southwest Jiaotong University, Chengdu 610031, China. ³Key Laboratory of High-speed Railway Engineering of Ministry of Education, Southwest Jiaotong University, 610031 Chengdu, China. ✉email: cdb1645@163.com

proposed a signal modification algorithm, a simple back-propagation artificial neural network architecture, which firstly improves the accuracy of the vertical contact force measured by strain gauges by 10% by eliminating the next significantly higher harmonic than that considered in the existing algorithms.

This paper attempts to propose an improved wheel-rail force measurement scheme using the resistive strain method, based on the current ground test scheme for wheel-rail force with single-point strain in rails, in order to obtain more accurate wheel-rail two-point contact position and load distribution. This paper proposes a method for setting strain gauges on the force measuring column and a corresponding decoupling scheme for the wheel-rail force of the bridge circuit to improve the accuracy of test results. To improve the economy of the test bench, it is necessary to reasonably determine the length of the measurement area and the density of force column deployment. The identification of two-point contact force distribution characteristics of the wheel-rail in the switch area is realized through simulated loading based on the established finite element model of the test bench. To improve the economy of the test bench, it is necessary to reasonably determine the length of the measurement area and the density of force column deployment. The identification of two-point contact force distribution characteristics of the wheel-rail in the switch area is realized through simulated loading based on the established finite element model of the test bench. It accurately measures the distribution of contact forces at two points of a static wheel track. The results can provide a test scheme for the theoretical research of wheel and rail damage in switch area. Due to the inherent complexity and logistical challenges involved in physically producing such rails, our experiments in this paper are currently limited to simulations performed using advanced software techniques.

Instrumentation of dynamometric switch

Structure of dynamometric switch

Switch is an important railway equipment that makes rolling stock branch from one track into another or cross another track, as shown in Fig. 1. When the train passes through the switch area, the wheels turn from one rail to another with discontinuous characteristics, which leads to a large impact effect that the wheel-rail relationship will become very complex. The dynamic interaction between the wheel and switch is severe, which increases the maintenance and repair investment and seriously affects the safety and smoothness of the vehicle through the switch¹².

Figure 2 shows several possible contact states when the wheel passes through different positions of the switch, including single-point contact (Fig. 2a), two-point contact (Fig. 2b and c) and three-point contact (Fig. 2d). The wheel-rail contact state shown in Fig. 2a and b is similar to the contact state of the rail in the main line, which has been studied in detail at present¹³. The wheel-rail contact state shown in Fig. 2c is bound to exist in the switch area when the vehicle passes from the sideway or straight direction. In the two-point contact condition, the transfer and distribution characteristics of wheel-rail forces are extremely complex¹⁴. The ground-based single-point wheel-rail force testing technique is already well established. In the 1930s, the rail strain-based method for testing wheel-rail force was developed with the invention and widespread use of resistive strain gauges. The strain-based method has become the mainstream test method¹⁵. Wheel-rail forces for international track testing are typically measured using strain gauges attached to the rails as the sensing element. The paper aims to identify the two-point contact situation in the switch area and propose an improved wheel-rail force ground testing scheme to provide experimental support for theoretical research in this field.

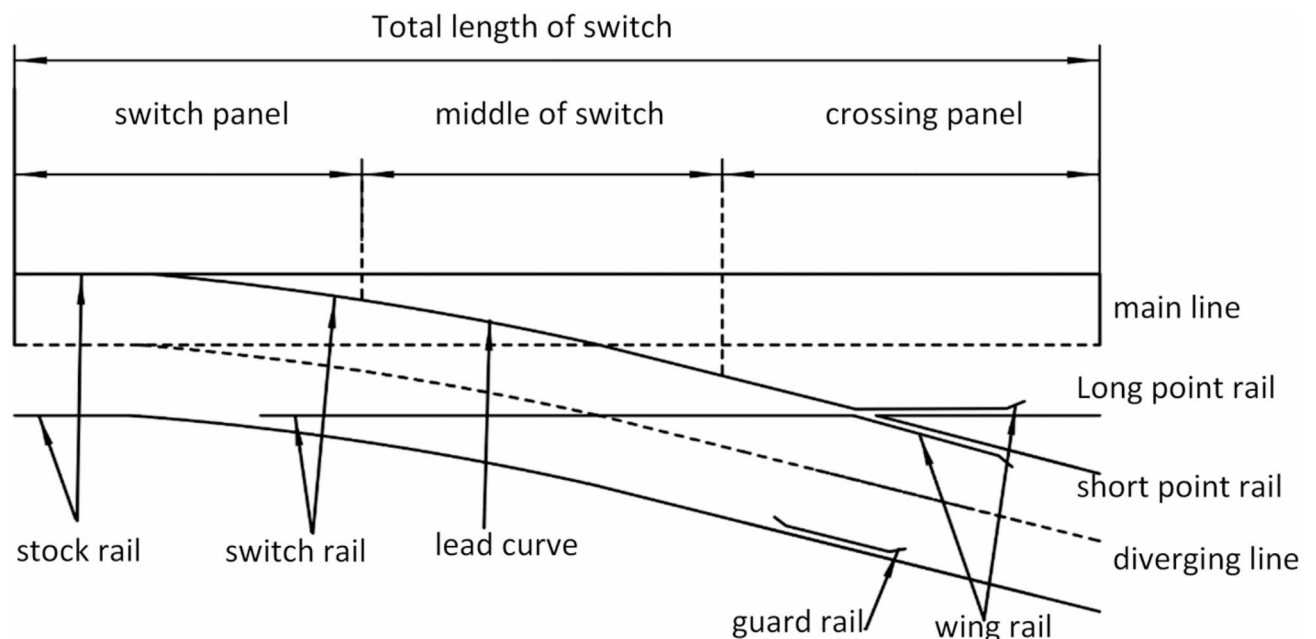


Fig. 1. Figure of switch area.

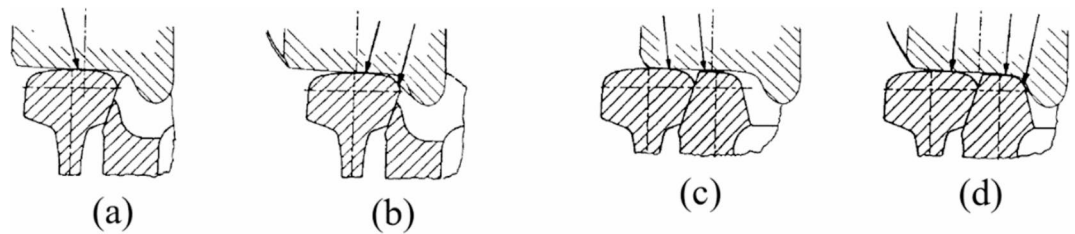


Fig. 2. Wheel-rail contact state in the switch area.

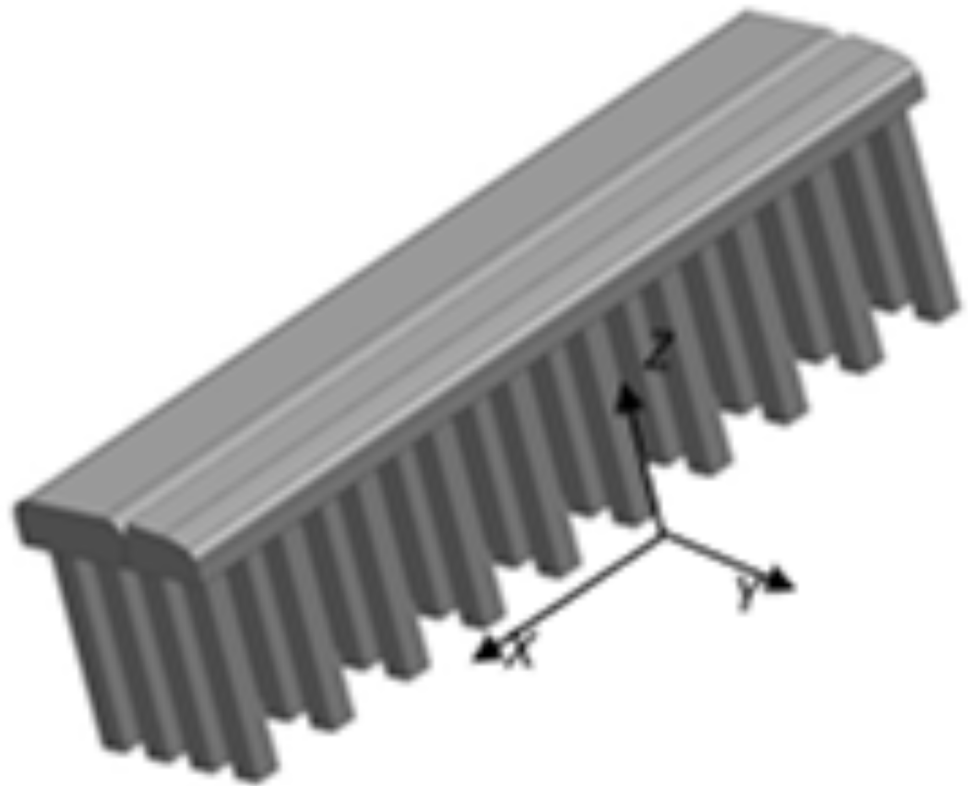
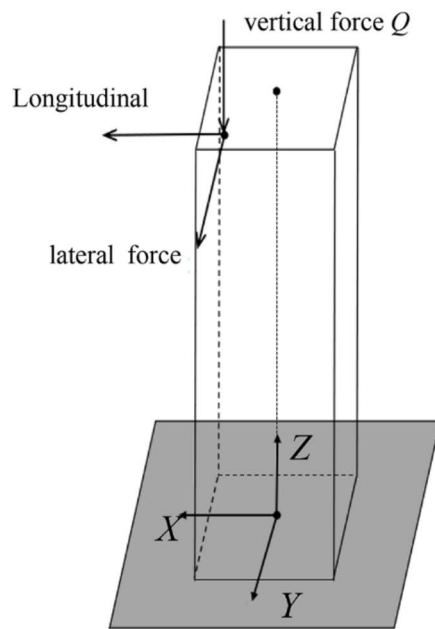


Fig. 3. Structure of dynamometric switch and layout of strain gauge.

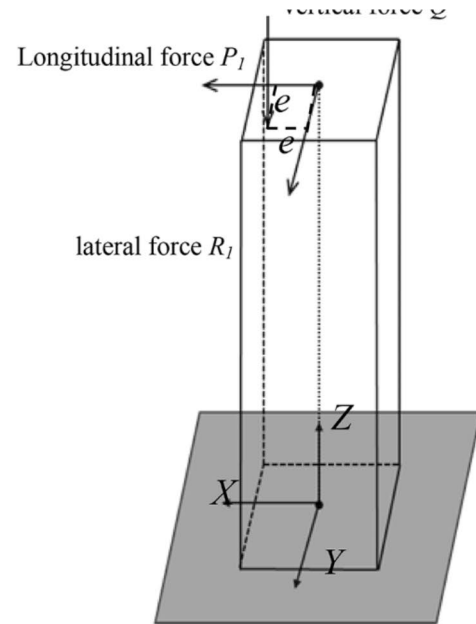
To accurately identify the wheel-rail force and its distribution, this paper proposes the theory of a new type of force-measuring column and evaluates its performance through software simulation. The dynamometric switch is designed according to the original switch, as shown in Fig. 3. The head dimensions of the basic rail and switch rail are retained, and the web plate of both are replaced with force-measuring columns. Due to the complexity and time-consuming nature of the actual production process for this rail, we have only evaluated it by finite elements at this time. In theory, the identification accuracy depends on the density of force-measuring columns. Considering the limited layout space and manufacturing cost of the dynamometric switch, the length of the dynamometric switch is 616 mm with 4 force-measuring columns laterally and 16 force-measuring columns longitudinally. The force column section is a square of 16 mm in length, and the size is 160 mm.

Force analysis of force measuring column

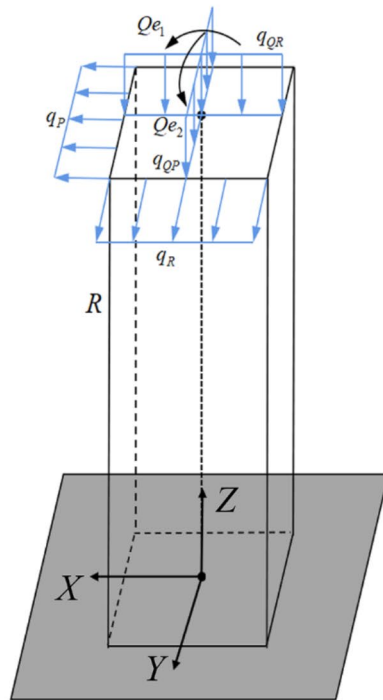
When the wheel rolls over the dynamometric switch, the force condition at any point on the top of force measuring column is shown in Fig. 4a. Since the rail top of the dynamometric switch is supported by multiple force-measuring columns, the torsional deformation of the force-measuring column along the Z-axis can be ignored. Under the action of wheel-rail force, the measuring columns mainly occur bending deformation along the x and y axes and compression deformation along the z axis. The vertical force Q, transverse force R, longitudinal force P and the position of the contact point determine its deformation. The column can be calculated for this principal basic deformation by simplifying the longitudinal or lateral force to the geometric



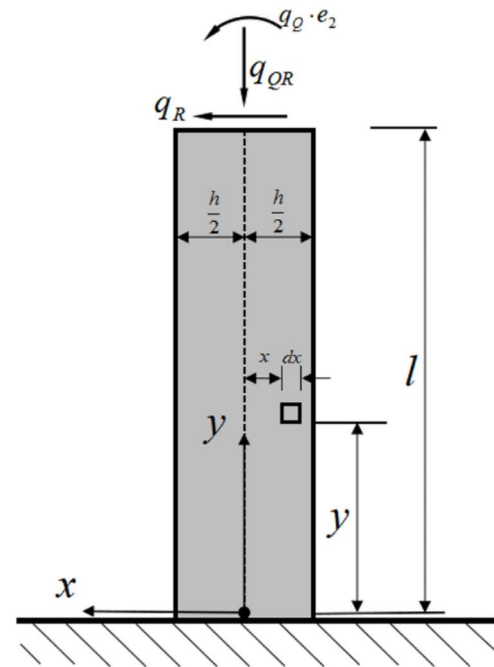
(a) Schematic diagram of force



(b) Schematic diagram of force projection



(c) equivalent force diagram



(d) cross-section force diagram in the X direction

Fig. 4. Stress state of the force column. (a) Schematic diagram of force. (b) Schematic diagram of force projection. (c) Equivalent force diagram. (d) Cross-section force diagram in the X direction.

center of the top of the column. To simplify the analysis, the forces in the three directions can be converted into uniform force and bending moment, as shown in Fig. 4b.

The vertical force Q will cause compression of force measuring column and bending along the X and Y directions due to the fact that the point of operation is not in the center of the top surface. To simplify the vertical force, the eccentric force Q is projected onto the x and y axes, as shown in Fig. 4a, with projection lengths of e_2 and e_1 in these two directions, respectively. At this point, Q can be resolved into the axial compressive force Q_1

and bending moments in the X and Y directions, denoted as $Q \cdot e_1, Q \cdot e_2$. Due to the force-measuring column's length and width being much smaller than its height, in the context of elasticity mechanics, the concentrated force on the top can be considered equivalent to the effect of a uniformly distributed load with the same direction of action. If Q is divided into two equal components of $Q/2$, these forces can be regarded as linearly distributed forces along the center of the top surface in the x and y directions, respectively, represented as q_{QP}, q_{QR} .

$$q_{QP} = q_{QR} = \frac{Q}{2h} \quad (1)$$

To facilitate the derivation of subsequent equations, the bending moments in both directions caused by the vertical force are also considered as uniform loads, denoted as $q_Q h \cdot e_1$ and $q_Q h \cdot e_2$, where, h is the side length of the square of the section of the force-measuring column. Longitudinal force P and transverse force R mainly cause bending deformation in two directions, which are respectively regarded as uniform load q_P, q_Q .

$$q_P = \frac{P}{h}, \quad q_Q = \frac{R}{h} \quad (2)$$

Since the force-measuring column section is square, its lateral and longitudinal forces are derived similarly, and only its lateral deformation is analyzed below. Figure 4c shows the force diagram of any section of the force column along the X direction. The stress function can be expressed as¹⁵:

The stress function satisfies:

$$\Phi = Axy + Byx^3 + Cx^3 + Dx^2 \quad (3)$$

$$\frac{\partial^4 \Phi}{\partial x^4} = 0, \quad \frac{\partial^4 \Phi}{\partial x^2 \partial y^2} = 0, \quad \frac{\partial^4 \Phi}{\partial y^4} = 0 \quad (4)$$

Satisfy the compatibility equation: $\frac{\partial^4 \Phi}{\partial x^4} + 2 \frac{\partial^4 \Phi}{\partial x^2 \partial y^2} + \frac{\partial^4 \Phi}{\partial y^4} = 0$

In the absence of body force, the components of stress in each direction can be found as:

$$\begin{cases} \sigma_x = \frac{\partial^2 \Phi}{\partial y^2} = 0 \\ \sigma_y = \frac{\partial^2 \Phi}{\partial x^2} = 6Bxy + 6Cx + 2D \\ \tau_{xy} = \tau_{yx} = -\frac{\partial^2 \Phi}{\partial x \partial y} = -A - 3Bx^2 \end{cases} \quad (5)$$

The constants A, B, C, and D should be calculated according to the boundary conditions.

There is no surface force at the right boundary of the thin plane ($x = h/2$), which must be satisfied:

$$(\sigma_x)_{x=h/2} = 0, \quad (\sigma_{xy})_{x=h/2} = 0 \quad (6)$$

The value of A can be found

$$A = -\frac{3}{4}h^2B \quad (7)$$

According to the boundary surface force is zero ($x = h/2$), the same A value can also be obtained.

According to the St. Venant principle, the equivalent stress boundary conditions at the upper boundary ($y = l$) of a thin plane are:

$$\begin{cases} \int_{-\frac{h}{2}}^{\frac{h}{2}} (\sigma_y)_{y=l} dx = -q_{QR} \\ \int_{-\frac{h}{2}}^{\frac{h}{2}} (\sigma_y)_{y=l} x dx = -q_Q \cdot e_2 \\ \int_{-\frac{h}{2}}^{\frac{h}{2}} (\tau_{xy})_{y=l} dx = -q_R \end{cases} \quad (8)$$

Substituting Eq. (5) into Eq. (8) gives

$$\begin{cases} D = -\frac{q_{QR}}{h} \\ Bl + C = -\frac{2q_Q \cdot e_2}{h^3} \\ Ah + \frac{h^3}{4}B = q_R \end{cases} \quad (9)$$

According to Eqs. (7) and (9)

$$\begin{cases} A = \frac{3q_R}{2h} \\ B = -\frac{2q_R}{h^3} \\ C = \frac{2(q_R l - q_Q \cdot e_2)}{h^3} \\ D = -\frac{q_{QR}}{h} \end{cases} \quad (10)$$

Substituting the values of the above constants A , B , C , and D into formula (5), the stress component can be obtained as

$$\begin{cases} \sigma_x = \frac{\partial^2 \Phi}{\partial y^2} = 0 \\ \sigma_y = \frac{\partial^2 \Phi}{\partial x^2} = -\frac{12q_R}{h^3}x(l-y) - \frac{12q_Q \cdot e_2}{h^3}x - \frac{q_{QR}}{h} \\ \tau_{xy} = \tau_{yx} = -\frac{\partial^2 \Phi}{\partial x \partial y} = \frac{6q_R}{h^3}x^2 - \frac{3q_R}{2h} \end{cases} \quad (11)$$

The relationship between stress (σ_x , σ_y and τ_{xy}) and load (q_{QR} , q_R , and Qe_2) on a thin plane is established by Eq. (11).

Method of longitudinal force and lateral force measurement

The strain gauges only respond to vertical compression and longitudinal bending caused by longitudinal force and vertical force. According to Eq. (11) can obtain the stress in the y -direction at any point on the force column at this time can be obtained as

$$\sigma_y = -\frac{12q_P}{h^3}x(l-y) - \frac{12q_Q \cdot e_1}{h^3}x - \frac{q_{QP}}{h} \quad (12)$$

According to Eq. (12), strain gauges at different mounting locations but the same longitudinal coordinate y have the same proportional coefficient for both longitudinal stress and bending moment. Therefore, when strain gauges at the same longitudinal coordinate but different transverse coordinates x are connected to form a circuit, they can output proportional stress. By selecting two sectional patches and two bridge outputs, one can determine the longitudinal force by obtaining longitudinal stress and bending moments with different proportional coefficients.

According to the rail waist bending moment difference method, to measure longitudinal forces, two pairs of strain gauges should be symmetrically and perpendicularly attached to two opposite surfaces in the x -direction. The study employs the double half-bridge bending moment difference method to test for longitudinal forces. The method involves specific patch locations and a bridge circuit, as shown in Fig. 5. Strain gauges 1 and 2 measure the bending moments at the section located $4/3l$ from the base surface, while strain gauges 5 and 6 are positioned at a distance $l/4$ from the base surface.

There is a linear relationship between stress and strain in the elastic deformation range of the force-measuring column,

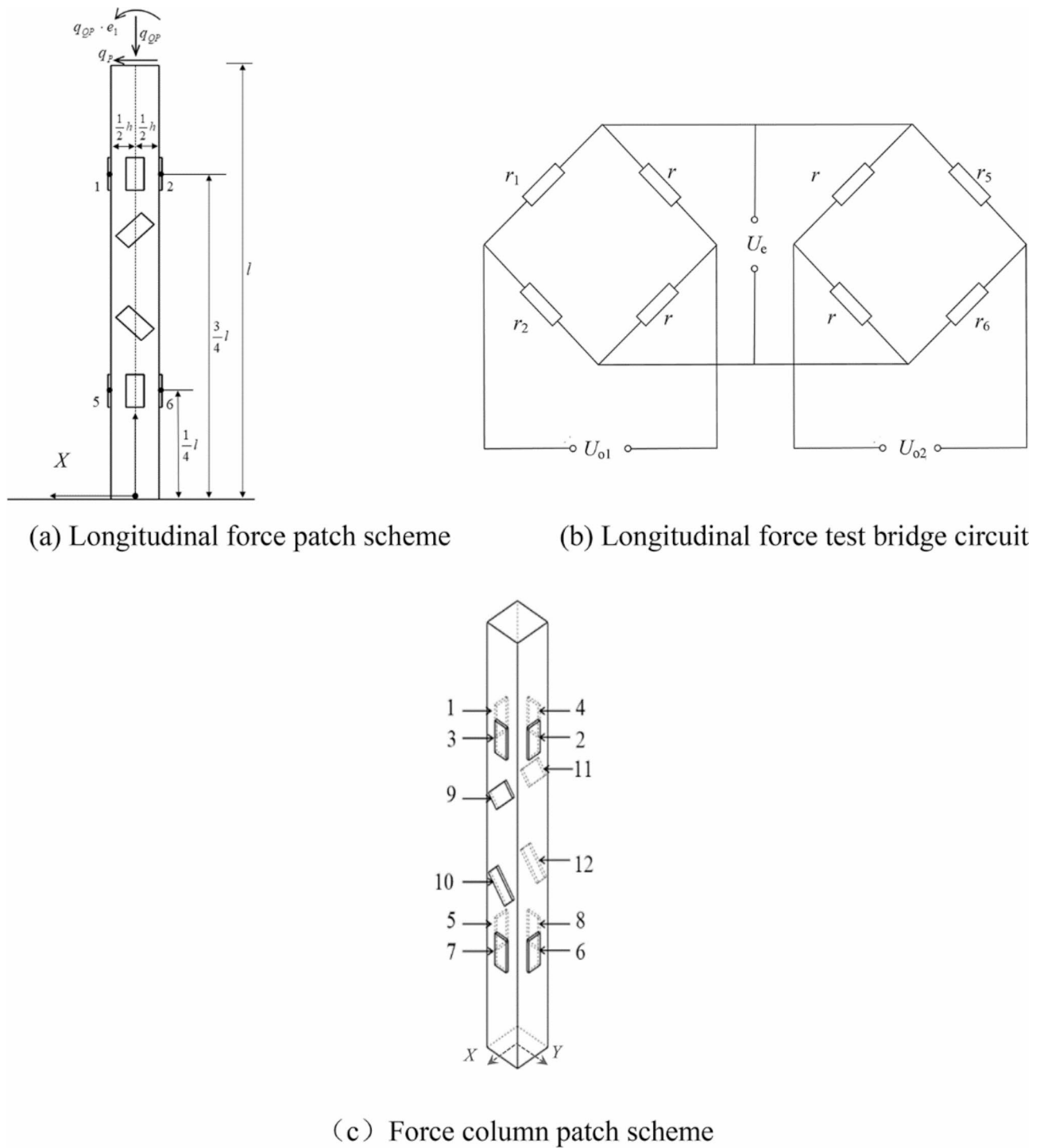


Fig. 5. Schematic diagram of longitudinal force test. (a) Longitudinal force patch scheme. (b) Longitudinal force test bridge circuit. (c) Force column patch scheme.

$$\begin{cases} \sigma_1 = -\frac{3l}{2h^2}q_P - \frac{6}{h^2}q_Q \cdot e_1 - \frac{q_{QP}}{h} \\ \sigma_2 = \frac{3l}{2h^2}q_P + \frac{6}{h^2}q_Q \cdot e_1 - \frac{q_{QP}}{h} \\ \sigma_5 = -\frac{9l}{h^2}q_P - \frac{6}{h^2}q_Q \cdot e_1 - \frac{q_{QP}}{h} \\ \sigma_6 = \frac{9l}{h^2}q_P + \frac{6}{h^2}q_Q \cdot e_1 - \frac{q_{QP}}{h} \end{cases} \quad (13)$$

$$\sigma = E\varepsilon \quad (14)$$

Where: E is the elastic modulus of the material. ε is the strain value, then the output of the two half bridges shown in Fig. 5b is

$$\begin{Bmatrix} U_{o1} \\ U_{o2} \end{Bmatrix} = \frac{3}{2} \cdot \frac{KU_e}{Eh^2} \begin{bmatrix} l & 4 \\ 3l & 4 \end{bmatrix} \begin{Bmatrix} q_P \\ q_Q \cdot e_1 \end{Bmatrix} \quad (15)$$

The equation demonstrates that the enhanced double bridge road technique can accomplish the decoupling of longitudinal forces between the wheel and rail.

The strain gauge used in the lateral force measurement is attached to the two faces in the Y direction, and its specific patch position and bridge design are the same as those of the longitudinal force. The lateral force test is similar to the longitudinal force test. It uses strain gauges 3, 4, 7 and 8, attached to the two faces in the Y direction. According to the derivation, the output of the two half bridges of the lateral force can be obtained as

$$\begin{Bmatrix} U_{o3} \\ U_{o4} \end{Bmatrix} = \frac{3}{2} \cdot \frac{KU_e}{Eh^2} \begin{bmatrix} l & 4 \\ 3l & 4 \end{bmatrix} \begin{Bmatrix} q_R \\ q_Q \cdot e_2 \end{Bmatrix} \quad (16)$$

Where, U_{o3} is the output voltage of the bridge where strain gauges No. 3 and No. 4 are located in Fig. 3b, and U_{o4} is the output voltage of the bridge where strain gauges No. 7 and No. 8 are located.

According to Eqs. (15) and (16), longitudinal force q_P and lateral force q_R of wheel and rail can be obtained. The relationship between the transverse load q_R and the bridge circuit outputs U_{o3} and U_{o4} has been established theoretically

Method of vertical force measurement

When the train is running on the track, examining some of the forces analyzed on four rail sleepers, the distribution of shear forces in the longitudinal section of the rail is shown in Fig. 6. Where, F_1, F_2, \dots, F_4 are four rail sleeper counterforces, S_r and S_l are the shear forces on the left and right sides of the wheel-rail force Q action point. It can be seen from Fig. 5 that the wheel-rail vertical force

$$Q = S_r + (-S_l) = |S_r| + |S_l| \quad (17)$$

Where, S_r, S_l is the rail shear force for wheel rail force action point of the left and right sides.

From Eq. (17), the magnitude of the vertical force Q is constant as the absolute value of the sum of the shear forces on both sides. Therefore, the $Q = S_r + (-S_l) = |S_r| + |S_l|$ vertical force of the wheel and rail can be obtained as long as the shear forces on both sides of the wheel-rail contact points between adjacent sleepers are measured. With the current testing technology, it is challenging to measure shear forces directly. This paper proposes measuring shear stresses to indirectly determine shear forces S_r, S_l . At the neutral axis of the horizontal section of the rail, there are no vertical or lateral stresses, only shear stress. Under pure shear conditions, the principal stress and the shear stress in the 45 degrees direction are equal. Therefore, the method of measuring the principal stress with strain gauges oriented at 45 degrees to the neutral axis of the rail web is used to determine the shear stress. Strain gauges are symmetrically arranged on the front and rear longitudinal faces of each measuring point, with two strain gauges on the same side (e.g. r9 and r10) symmetrically positioned relative to the neutral axis of the measuring point and angled at 45 degrees to the neutral plane.

The strain values of two strain gauges (r_9, r_{10} as examples) on the same column surface are

$$\begin{cases} \varepsilon_9 = \frac{\varepsilon_x + \varepsilon_y}{2} + \frac{\varepsilon_x - \varepsilon_y}{2} \cos 2\theta_1 + \frac{\gamma_{xy}}{2} \sin 2\theta_1 \\ \varepsilon_{10} = \frac{\varepsilon_x + \varepsilon_y}{2} + \frac{\varepsilon_x - \varepsilon_y}{2} \cos 2\theta_2 + \frac{\gamma_{xy}}{2} \sin 2\theta_2 \end{cases} \quad (18)$$

In the above formula, $\varepsilon_9, \varepsilon_{10}$ are the strains of strain gauge 9 and 10 respectively, $\varepsilon_x, \varepsilon_y$ are the strains in the direction of the x and y axes of the coordinate system respectively; θ is the angle between the strain gauge and the neutral plane; γ_{xy} is the shear strain in the space coordinate system which can be expressed as

$$\gamma_{xy} = \frac{2(\varepsilon_9 - \varepsilon_{10}) - (\varepsilon_x - \varepsilon_y)(\cos 2\theta_1 - \cos 2\theta_2)}{\sin 2\theta_1 - \sin 2\theta_2} \quad (19)$$

When the strain gauges are symmetric about the neutral plane, i.e., $\theta_1 = -\theta_2 = 45^\circ$, then

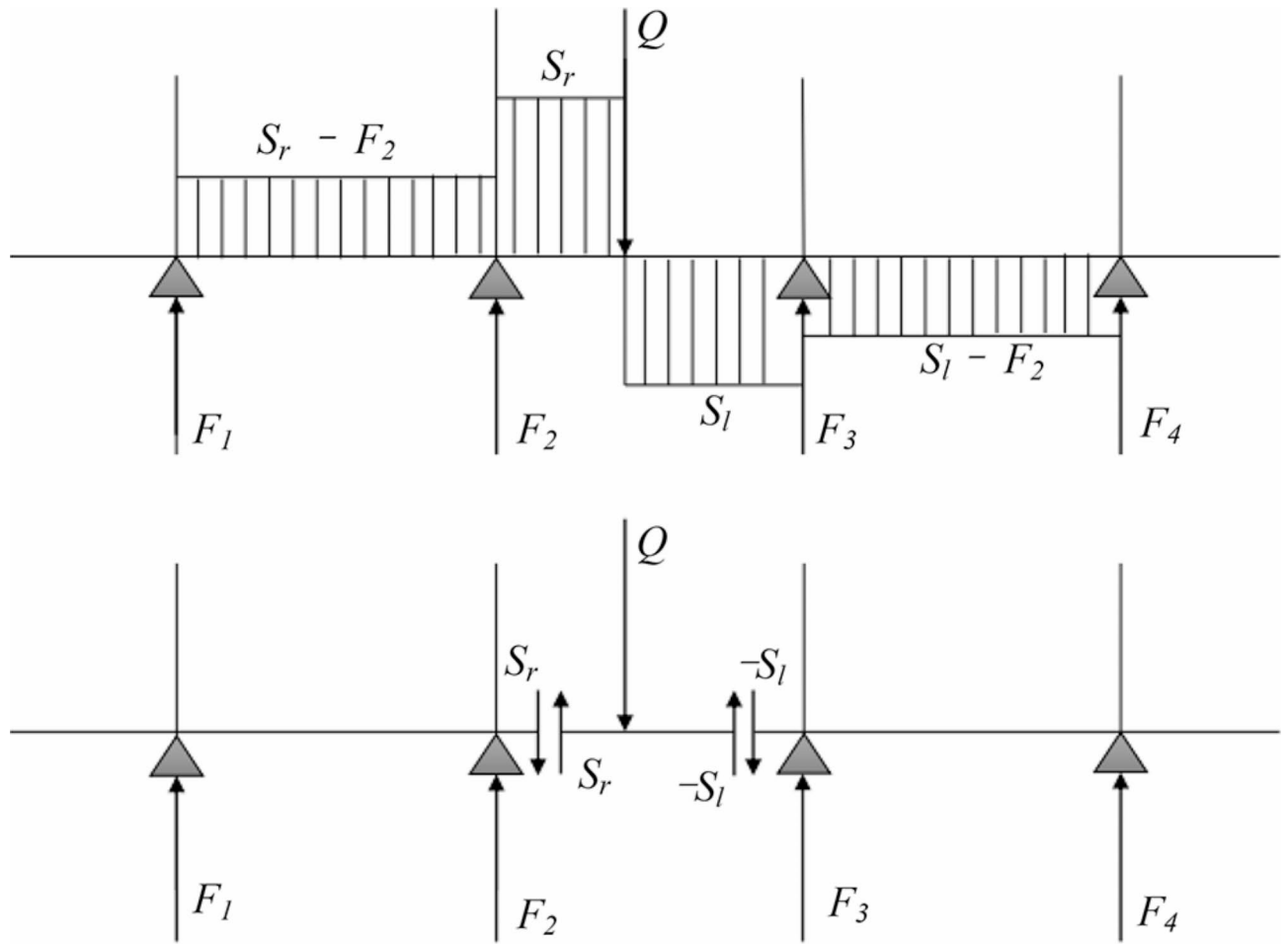


Fig. 6. Schematic diagram of wheel track vertical force test¹⁶.

$$\gamma_{xy} = \varepsilon_9 - \varepsilon_{10} \quad (20)$$

The value of $\varepsilon_9 - \varepsilon_{10}$ can be obtained through the electric bridge output. According to the elastic modulus of the rail, the neutral layer shear stress τ in the strain gauge arrangement cross-section can be calculated from the shear strain γ_{xy} . The relationship between shear stress and shear force can be determined from the shear stress Eq. (21) to obtain the shear force S .

$$\tau = \frac{G_z^*}{I_z b} \cdot S \quad (21)$$

Where, τ is the shear stress, S is the shear force on the cross-section, G_z^* is the static moment of the cross-section outward from the shear calculation point to the neutral axis, I_z is the moment of the cross-section to the neutral axis, b is the thickness of the section.

According to the above principles, the strain gauges shown in Fig. 7b can be used to measure the rail shear stress by the bridge when the wheel passes through. To measure shear forces in different cross-sections, eight strain gauges were used to form a full bridge circuit. And the vertical force Q of the wheel/rail can be obtained by calibration. The bridge excitation voltage is U_e , the sensitivity coefficient of the strain gauge is K , and the initial resistance value of the strain gauge is R , then the output voltage of the bridge is

$$U_{os} = U_e \frac{((2r + \Delta r_9 + \Delta r_{9'}) (2r + \Delta r_{11} + \Delta r_{11'}) - (2r + \Delta r_{12} + \Delta r_{12'}) (2r + \Delta r_{10} + \Delta r_{10'}))}{(4r + \Delta r_9 + \Delta r_{10} + \Delta r_{9'} + \Delta r_{10'}) (4r + \Delta r_{11} + \Delta r_{12} + \Delta r_{11'} + \Delta r_{12'})} \quad (22)$$

Omit the higher-order small quantity in Eq. (5)

$$U_{os} = \frac{KU_e}{8} [(\varepsilon_9 + \varepsilon_{9'} + \varepsilon_{11} + \varepsilon_{11'}) - (\varepsilon_{10} + \varepsilon_{10'} + \varepsilon_{12} + \varepsilon_{12'})] = -\frac{KU_e G_z^*}{2EI_z h} Q \quad (23)$$

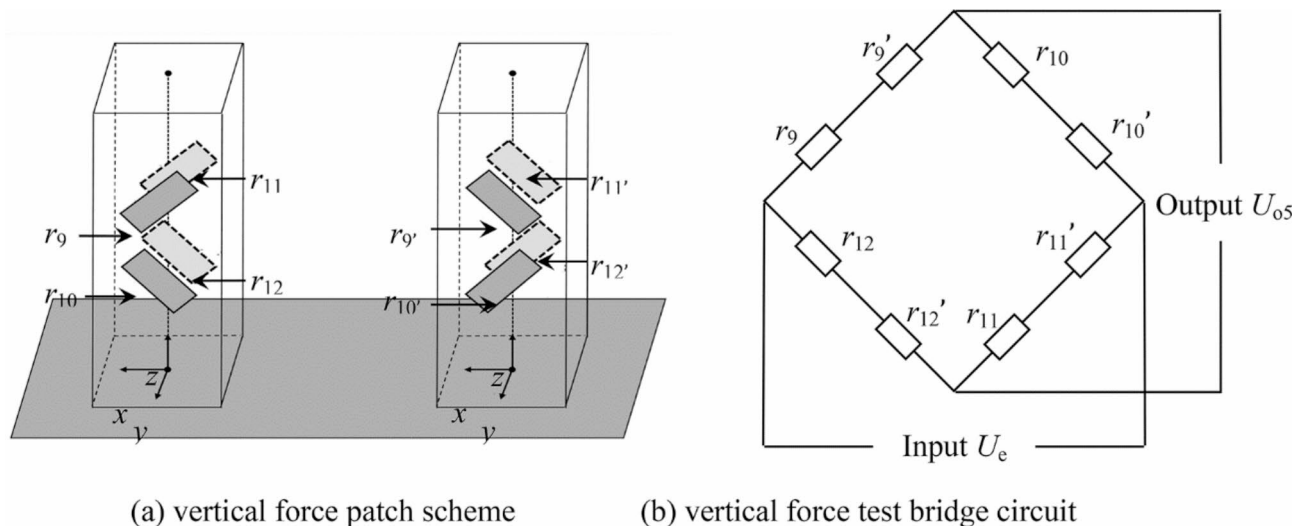


Fig. 7. measurement of wheel/rail vertical force. (a) vertical force patch scheme (b) vertical force test bridge circuit.

Wheel-rail contact stress identification

Horizontal force calibration

Although Eqs. (15), (16), and (23) give the relationship between the forces in each direction and the output voltage of the test bridge, it is difficult to obtain the exact wheel-track forces directly in practical engineering because of the material and structural parameters included in the equations. Using the calibrating method to obtain the relationship between the wheel-rail force and strain in each direction is a common engineering method. In this section, the finite element method is used to calculate the relationship between the strain value and wheel-rail force, the calibration of the dynamometric switch is completed, and the difference between the calibration and the theoretical value is compared.

Because the output voltage of the bridge in the theoretical calculation is obtained from the material strain value of each strain gauge area, for the convenience of subsequent discussion, the output voltage value is replaced by the strain value. By substituting $h = 16$ mm, $l = 160$ mm, $E = 2.1 \times 10^{11}$ into Eq. (15), the relation between the strain value ε of the strain gauge and load can be obtained as follows,

$$\begin{Bmatrix} \varepsilon_2 - \varepsilon_1 \\ \varepsilon_6 - \varepsilon_5 \end{Bmatrix} = 1 \times 10^{-6} \cdot \begin{bmatrix} 0.5590 & 13.9509 \\ 1.6741 & 13.9509 \end{bmatrix} \begin{Bmatrix} P \\ Qe_1 \end{Bmatrix} \quad (24)$$

Thus, a direct relation between strain and load is obtained.

Express the coefficient matrix in Eq. (24) as \mathbf{k} ,

$$\begin{Bmatrix} \varepsilon_2 - \varepsilon_1 \\ \varepsilon_6 - \varepsilon_5 \end{Bmatrix} = 1 \times 10^{-6} \cdot \begin{bmatrix} k_{11} & k_{12} \\ k_{13} & k_{14} \end{bmatrix} \begin{Bmatrix} P \\ Qe_1 \end{Bmatrix} \quad (25)$$

The strain value of the strain gauges with different P and Qe_1 can be obtained using the finite element method. The matrix coefficient can be solved by Eq. (25). A constant torque (40 Nm in this paper) is applied to the top of the force-measuring column under total constraints imposed on the bottom of the column. The longitudinal force P value is changed from 1 to 4 kN, then the curves of $\varepsilon_2 - \varepsilon_1$ and $\varepsilon_6 - \varepsilon_5$ change with P can be obtained as shown in Fig. 8a, of which the gradient is the coefficient k_{11} and k_{13} . Similarly, fixing the value of P (2 kN in this paper), varying the value of Qe from 0 to 80 Nm can get curves of $\varepsilon_2 - \varepsilon_1$ and $\varepsilon_6 - \varepsilon_5$ with Qe , then the coefficient k_{12} , k_{14} can be obtained.

The coefficient matrix \mathbf{k} obtained according to Fig. 8 is

$$\mathbf{k} = \begin{bmatrix} 0.5202 & 13.0065 \\ 1.5606 & 13.0050 \end{bmatrix} \quad (26)$$

The matrix differs from Eq. (24) by about 7.31%, which is mainly for the simplification of the equation. It is recommended to use the coefficient matrix \mathbf{k} obtained by text calibration.

The strain gauge bridge for the lateral force is identical to the longitudinal force, and its coefficient matrix is also the same.

Vertical force calibration

Since the vertical force test bridge spans the different measuring columns, a single force measuring column cannot be used to calibrate the bridge coefficient. This study uses the whole dynamometric switch model shown in Fig. 3 to calibrate the vertical force. Full restraint is used below the columns, and vertical force Q is applied

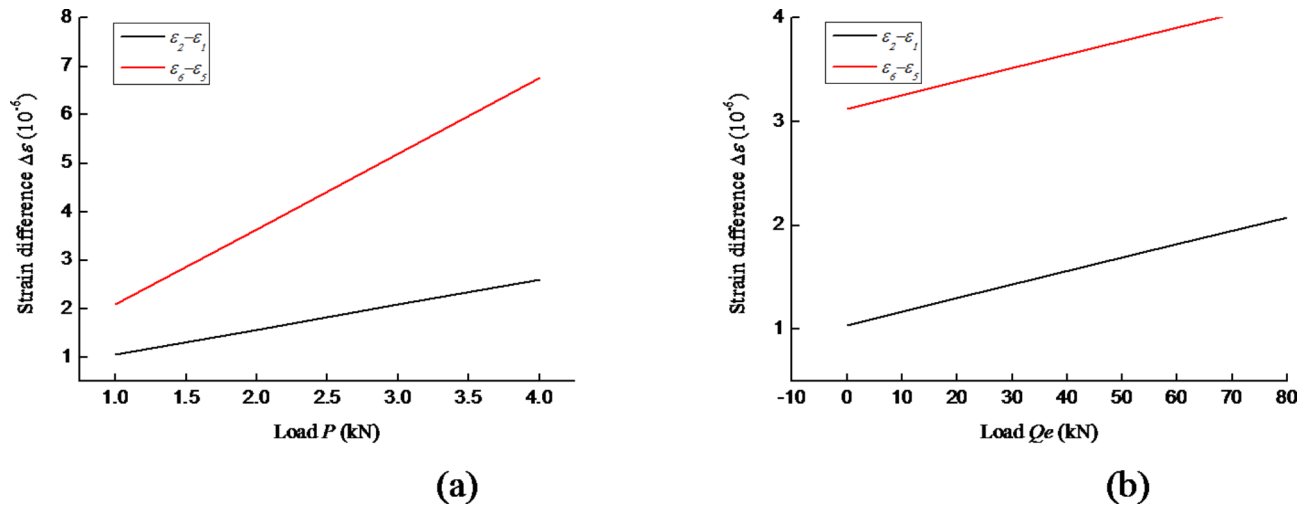


Fig. 8. Response of longitudinal bridge strain difference to load. (a) Variation of strain difference with load P . (b) Variation of strain difference with load Qe .

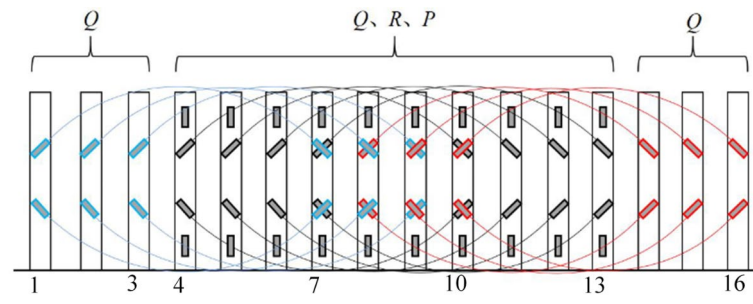


Fig. 9. Strain gauge bridge connection diagram.

to the middle of the rail, then, the strain difference $(\epsilon_9 + \epsilon_{9'} + \epsilon_{11} + \epsilon_{11'}) - (\epsilon_{10} + \epsilon_{10'} + \epsilon_{12} + \epsilon_{12'})$ of the test bridge can be obtained. The relationship between strain difference and load is shown in Fig. 8, which shows that the strain difference is basically linear with the load, and the scale factor is about -8.6532×10^{-8} . Then Eq. (23) is converted into

$$[(\epsilon_9 + \epsilon_{9'} + \epsilon_{11} + \epsilon_{11'}) - (\epsilon_{10} + \epsilon_{10'} + \epsilon_{12} + \epsilon_{12'})] = -8.6532 \times 10^{-8} \cdot Q \quad (27)$$

The wheel-rail vertical force Q can be obtained from Eq. (27) based on the strain response of the bridge, the wheel-rail contact point location e_1 can be obtained by Eq. (25), as well as e_2 . Thus, the wheel-rail contact stress distribution can be identified.

Identification of wheel-rail contact force distribution

Force measuring test model

The structure of force measuring test

The finite element model of the switch area test bench consists of two parts: the rail head part and the column part. The force measuring column is required to perform patch testing. Due to the unique structure of the switch area, it is also necessary to consider the contact problem between the point rail and the stock rail when modelling. The analysis of the shear method for testing the vertical force in 2.4 shows that the measurement of the vertical force requires eight strain gauges to be affixed to two opposite columns. According to the relevant research data, the vertical force measured when the distance between two groups of strain gauges is 240 mm is subject to the least interference¹⁷, so this paper selects the spacing of each group of columns as 240 mm. Since the vertical force test bridge circuit has a certain span along the longitudinal direction, in order to obtain more accurate identification results, the test position of the vertical force is the same as that of the lateral and longitudinal forces, and at the same time, in order to reduce the number of forces measuring columns, 16 force measuring columns are arranged in each row. To ensure that the 10 vertical force data correspond to the middle 10 columns, refer to the patch scheme shown in Fig. 9. Columns 1–3 and 14–16 are solely used to calculate the vertical force Q at the top of the columns. Meanwhile, columns 4–13 are used to calculate the vertical, transverse, and longitudinal forces. Columns 7–10 are used twice to test the vertical force.

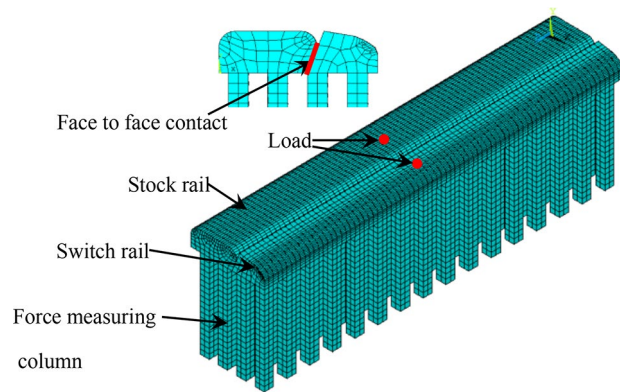


Fig. 10. Finite element model of dynamometric switch.

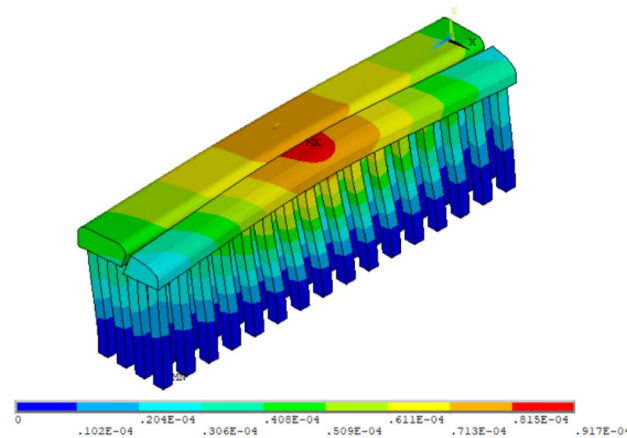


Fig. 11. Strain of dynamometric switch.

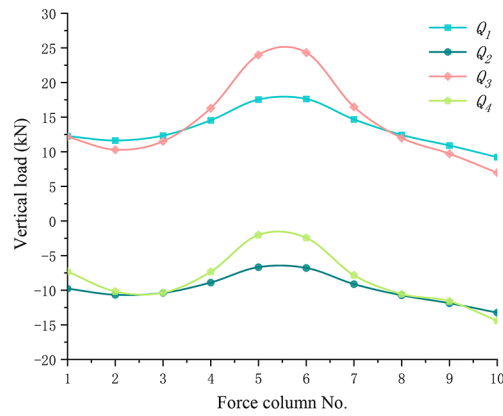
The finite element model of force measuring test

The dynamometric switch was modeled using ANSYS software¹⁸, as shown in Fig. 10. The material elastic modulus is 2.1×10^{11} Pa and Poisson's ratio of 0.3. The model used a hexahedral mesh, the finite element model of the rail head part and the force column under the rail head part of the contact position of the duplicate nodes were merged, the basic rail and the tip rail of the test bench are modeled separately. To ensure that there is no separation of the penalty function contact algorithm is used. The face-to-face contact unit is established between the stock rail and switch rail, and the friction coefficient is 0.3. The full constraint is applied at the bottom of the model, and the wheel-rail force is applied to the rail surface as a concentrated force.

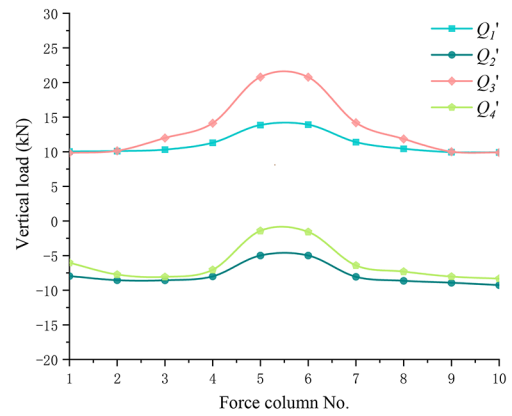
Since there is a certain span along the longitudinal side of the vertical force test bridge, the test position of the vertical force should be consistent with that of the transverse and longitudinal forces to obtain more accurate identification results. The test bridge with the wheel-rail action point in the center of the vertical bridge was selected for the analysis of contact force identification. According to the above results, only the wheel-rail vertical force can be identified within the range of 3 force-measuring columns along the longitudinal direction, the range of 10 force-measuring columns in the middle is the area of identification of the three-way force, and the position of the wheel-rail action point. In this research, when the load is applied near the middle of the force-measuring rail, the magnitude of the force applied on the sharp rail is vertical force = 50 kN, transverse force, R_t = 40 kN, longitudinal force, P_t = 25 kN, and the magnitude of the force applied on the basic rail is vertical force, Q_b = 408 kN, transverse force, R_b = 30 kN, longitudinal force, P_b = 15 kN. The strain of the dynamometric switch model can be obtained through simulation calculation, as shown in Fig. 11.

Contact force identification

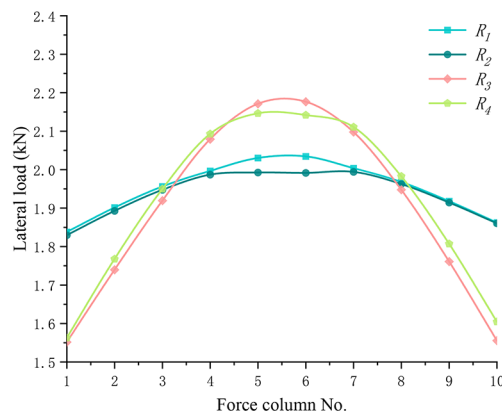
The strain value of other corresponding positions of the strain gauge on all the force-measuring column can be extracted, and then, the force and the offset can be solved according to Eqs. (24) and (26), as shown in Fig. 11. The abscissa is the longitudinal number of the columns, and the subscript number in the label is the lateral number of the columns, where rows 1 and 2 are located below the switch rail, and rows 3 and 4 are located below the stock rail. The lateral bending of the rail due to the lateral force of the wheel-rail causes compression on one side and tension on the other side of the force-measuring column below the switch rail and stock rail, which leads to the negative vertical force on the two rows of force-measuring columns as shown in Fig. 12a. The force



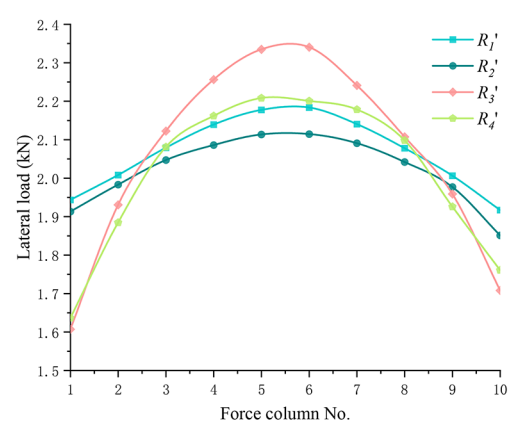
(a) Vertical force distribution decoupled



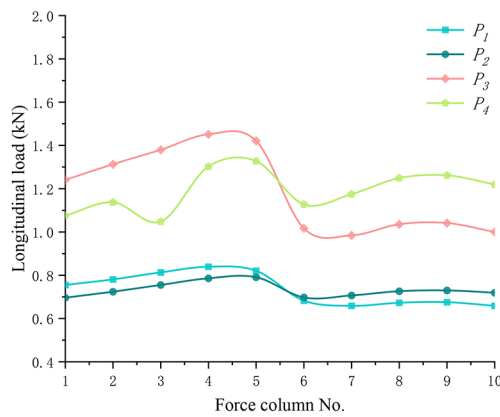
(b) Vertical force distribution on the column



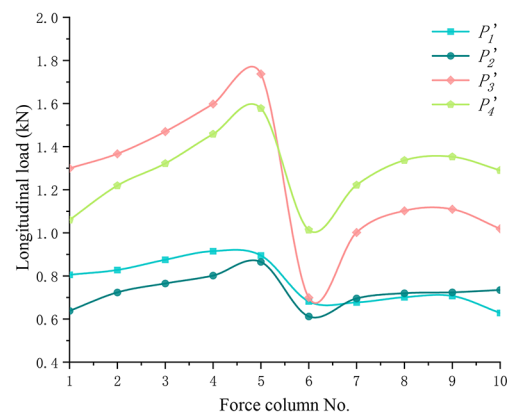
(c) Lateral force distribution decoupled



(d) Lateral force distribution on the column



(e) Longitudinal force distribution decoupled



(f) Longitudinal force distribution on the column

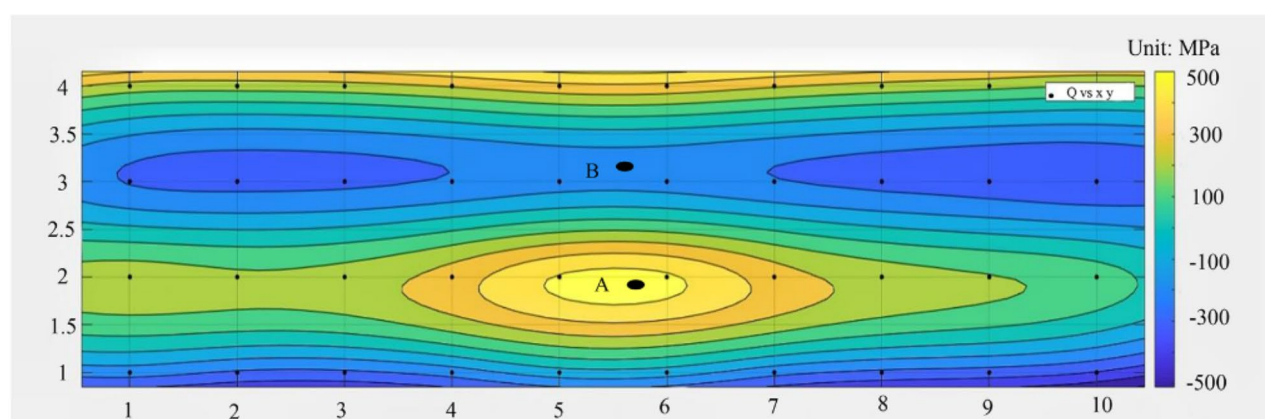
Fig. 12. Comparison of the decoupled and extracted forces. (a) Vertical force distribution decoupled. (b) Vertical force distribution on the column. (c) Lateral force distribution decoupled. (d) Lateral force distribution on the column. (e) Longitudinal force distribution decoupled. (f) Longitudinal force distribution on the column.

distribution on the railhead can be obtained by applying the cubic spline differences of the force on the columns shown in Fig. 12. As can be seen in Fig. 12, the wheel-rail force distribution curve obtained indirectly by the decoupling scheme is in good agreement with the wheel-rail force distribution curve obtained directly by the finite element model of the test bench in the switch area, which indicates that the decoupling scheme is more

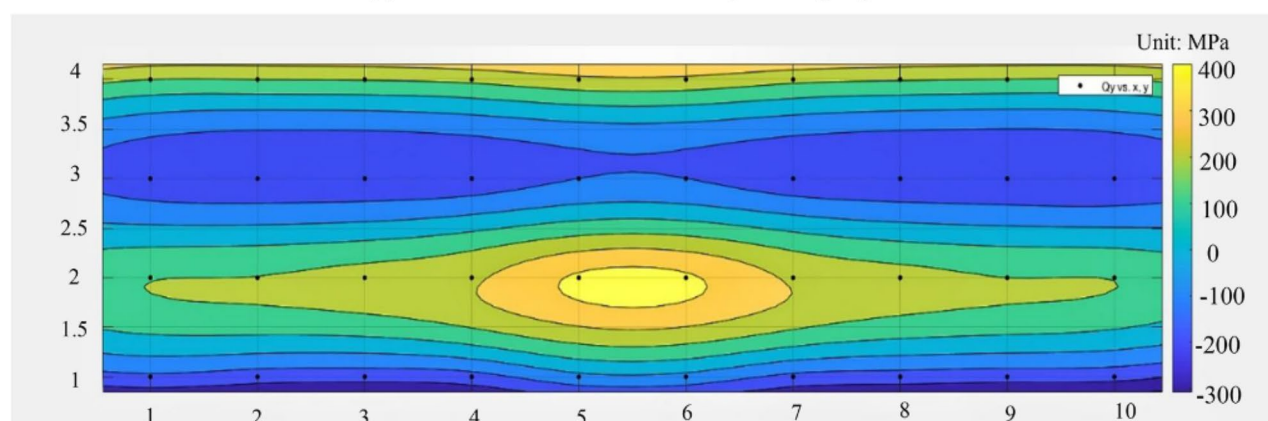
effective. The result of the vertical force is the best, and its waveform and magnitude are close to the waveform and magnitude of the vertical force distribution obtained directly; the waveform of the lateral force obtained by the test is close to that obtained by the finite element, and the difference of the lateral force distribution on different rails is also more obvious.

The distribution states of the forces on the railhead are given in Figs. 13, 14 and 15. It can be seen that the load distribution on the railhead is consistent with the load distribution obtained by finite element, and the size is slightly different. The longitudinal deviation is approximately 4.4 mm, and the lateral deviation is roughly 3.2 mm. Figure 13 displays a maximum compressive stress on the switch rail at peak point A, situated near the loading position. Affected by the slope between the switch rail and the stock rail, the vertical load of the stock rail is partly supported by the switch rail and is affected by the transverse force from the switch rail. Thus, the load at the bottom of the railhead is dominated by tensile stress. The vertical load on the stock rail will offset the tension at the bottom of the railhead, so load point B, with the smallest local tension, can be considered as the load point of the railhead, with longitudinal and transverse deviations are about 6.3 mm and 4.6 mm respectively. As shown in Fig. 13, the actual vertical load in the measurement exceeds the analyzed 10 force measuring columns range, resulting in a large calibration factor and strain gauge identification load. The load value identified by strain gauges is about 87.2 MPa larger than this obtained by finite element analysis. Because the load to be identified is the total load in the entire identification area, although the load value of a single column is too large, it does not include the total column in the full load range, so the total load value identified by this method does not deviate seriously from the actual value. The identified total vertical load value is 94.6568 kN, and the deviation rate is 5.34%, closer to the actual load.

The lateral load distribution of the railhead identified by strain gauges is very similar to the trend and value of the finite element calculation results, as shown in Fig. 14. A local stress maximum point exists near the point of load acting on the switch rail and the stock rail respectively, point C and point D. Due to the mutual extrusion between the switch rail and stock rail, the load position of railhead will offset from the load distribution at the bottom of railhead, and the transverse offset cannot be ignored. The longitudinal load distribution shown in Fig. 15. It shows that the identified results by strain gauges are similar to the finite element calculations. However,



(a) Load distribution identified by strain gauges



(b) Load distribution obtained by finite element method

Fig. 13. Vertical load distribution of railhead. (a) Load distribution identified by strain gauges. (b) Load distribution obtained by finite element method.

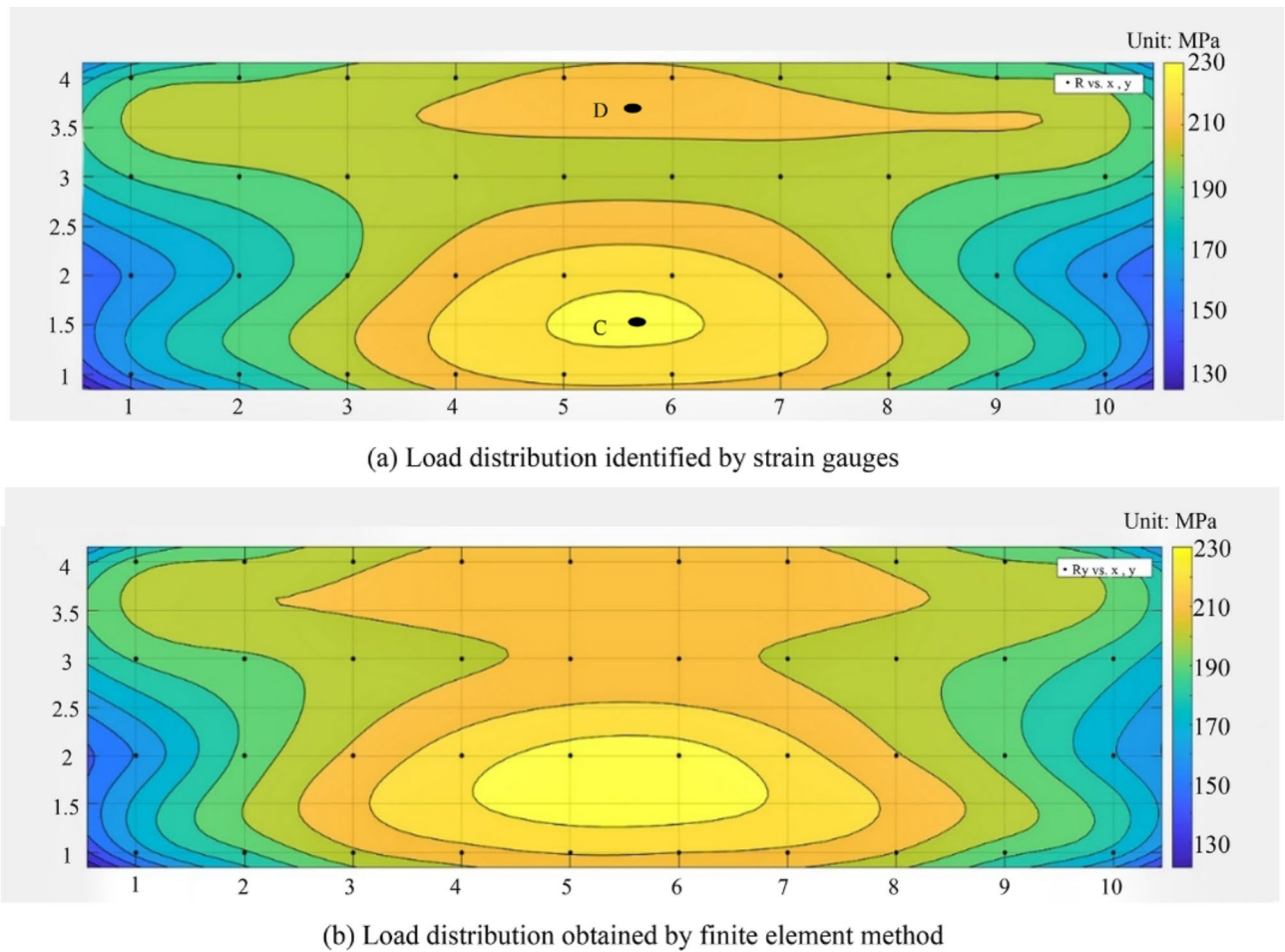


Fig. 14. Lateral load distribution of railhead. (a) Load distribution identified by strain gauges. (b) Load distribution obtained by finite element method.

due to the longitudinal extrusion of the material, it is difficult to identify the load action position according to the longitudinal force distribution characteristics.

The load value applied to the railhead can be obtained by summing the load value at the bottom of the railhead. However, due to the interaction between the switch rail and the stock rail, it is difficult to obtain the accurate load value at the two contact points. Figure 16 shows the forces on the railhead, where, Q_p, Q_b, R_p, R_b are distribution loads of the two-point contact forces to be identified on the railhead, Q_1-Q_4 are vertical support forces of the columns, R_1-R_4 are the lateral support forces of the column, Q_n, Q_m, R_n, R_m are the interaction forces between the switch rail and stock rail, e_1-e_4 are the lateral offsets of the vertical force of each column, L_1, L_2 are the distances from the interaction force position between the switch rail or the stock rail to the wheel-rail contact point, L_3 is the nominal thickness of the railhead. According to the balance of force and moment, each force must satisfy Eq. (28), and the load value on the switch rail and stock rail can be obtained, as shown in Table 1. Where the longitudinal force is obtained by directly adding the longitudinal force of each column in Fig. 14. From the value of identified forces in each direction, except the longitudinal force is smaller, the other force is bigger than the actual value, and the deviation rate of each value is within 10%. The error mainly comes from the approximate estimation of each parameter, including the deviation of the contact point identified by the vertical load distribution at the bottom of the rail, the approximate replacement of the height of the contact point to the bottom of the rail by the railhead thickness value, and the neglect of the friction between the contact surface of the switch rail and stock rail.

$$\left\{ \begin{array}{l} Q_t = Q_1 + Q_2 - Q_m \\ Q_b = Q_3 + Q_4 + Q_n \\ R_t = R_m + R_1 + R_2 \\ R_b = R_4 + R_3 - R_n \\ R_t L_3 + Q_b e_1 + Q_m L_1 = Q_2 e_2 + R_m L_1 \\ R_b L_3 + Q_3 e_3 + Q_n L_2 + R_n L_1 = Q_4 e_4 \\ R_n = R_m \\ Q_n = Q_m \end{array} \right. \quad (28)$$

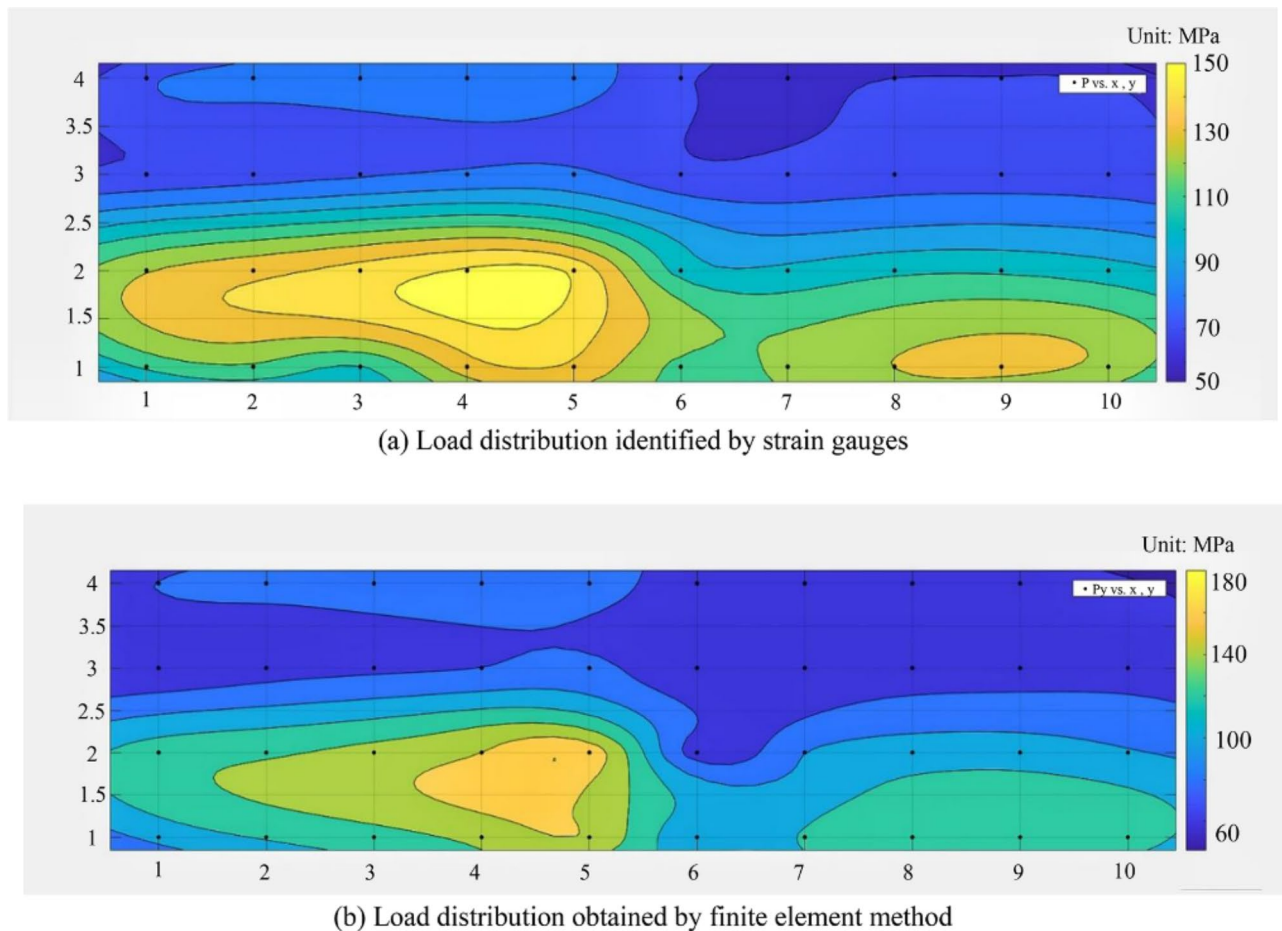


Fig. 15. Longitudinal load distribution of railhead. (a) Load distribution identified by strain gauges. (b) Load distribution obtained by finite element method.

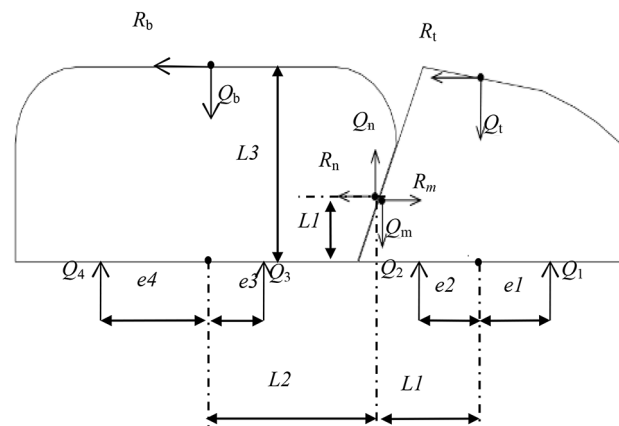


Fig. 16. Schematic diagram of railhead forces.

force	Q_t	Q_b	R_t	R_b	P_t	P_b
Identify the value /kN	52.8696	41.7872	43.52 28	31.0227	23.8047	14.6859
Deviation rate /%	5.74	4.47	8.81	3.41	4.78	2.09

Table 1. Results of two-point contact force identification.

Conclusion

For the problem that it is difficult to calculate and test the switch area's two-point contact state, this study presents an efficient and accurate method for inversing wheel-rail forces. A strain gauge bridge grouping scheme was developed that employs the rail waist gap method and the stress difference method. A dynamometric switch with a discrete force-measuring column supporting the railhead was developed. According to the structure and force characteristics of the dynamometric switch, the bridge arrangement for load identification was introduced, and the decoupling method of the force was derived. The finite element method was used to calibrate each bridge and simulate the stress state of the dynamometric switch under two-point contact conditions. The strain values in the area where the strain gauges were located were extracted, and the load distribution on the railhead and the two-point contact force were identified according to the force decoupling equation.

The results show that the load distribution of the railhead identified by the strain gauge is consistent with the finite element analysis results, which can reflect the force state of the railhead. The two-points contact positions on the railhead can be accurately identified according to the vertical load distribution. The lateral load distribution of the railhead can clearly reflect the two-point contact state, but due to the interaction between the switch rail and stock rail, there is a large deviation in the identification of the load position on the railhead. According to the structure size and force relationship of the dynamometric switch, the load value in each direction on the railhead can be identified, and the error is within 10%, which can meet the engineering test requirements.

The dynamometric switch technology provides a feasible test verification scheme for the theory of two-point contact in the switch area and a practical engineering technology for monitoring of wheel and rail in the switch area.

Data availability

The datasets generated and analyzed during the current study are available from the corresponding author on reasonable requests.

Received: 18 August 2024; Accepted: 6 January 2025

Published online: 29 January 2025

References

- Kalker, J. A fast algorithm for the simplified theory of rolling contact. *Veh. Syst. Dyn.* **11**(1), 1–13 (1982).
- An, B. & Wang, P. A wheel–rail normal contact model using the combination of virtual penetration method and strip-like Boussinesq's integral. *Veh. Syst. Dyn.* **61**(6), 1583–1601 (2023).
- Shen, Z., Hedrick, J. K. & Klkins, J. A. A comparison of alternative creep force models for rail vehicle dynamic analysis. *Veh. Syst. Dyn.* **12**, 79–83 (1983).
- Gómez, E. et al. Railway dynamometric wheelsets: a comparison of existing solutions and a proposal for the reduction of measurement errors. In *Proceedings of the 1st International Workshop on High-Speed and Intercity Railways*, vol. 2 261–284 (2012).
- Gómez, E., Giménez, J. & Alonso, A. Method for the reduction of measurement errors associated to the wheel rotation in railway dynamometric wheelsets. *Mech. Syst. Signal. Process.* **25**(8), 3062–3077 (2011).
- Matsumoto, A. et al. A new measuring method of wheel–rail contact forces and related considerations. *Wear* **265**(9–10), 1518–1525 (2008).
- Gong, X. et al. Research on continuous measurement method for wheel-rail forces and validation with 1:5 scale roller rig test. *J. Mech. Eng.* **56**(2), 184–191 (2022).
- Bižić, M. & Petrović, D. Design of instrumented wheelset for measuring wheel-rail interaction forces. *Metrol. Meas. Syst.* **563**, 579 (2023).
- Kanehara, H. Takehiko Fujioka. Measuring rail/wheel contact points of running railway vehicles. *Wear* **253**, 275–283 (2002).
- Lan, C. et al. Research on inversion of wheel-rail force based on neural network framework. *Eng. Struct.* **304**, 117662 (2024).
- Ropalkar, O. S. et al. Improved estimation of rail–wheel contact forces from instrumented wheel-set data through higher harmonic cancellation and a back-propagation neural network scheme. *Eng. Appl. Artif. Intell.* **119**, 105811 (2023).
- Gurule, S. & Wilson, N. Simulation of wheel/rail interaction in turnouts and special trackwork. In *16th IASD Symposium Pretoria, South Africa* 35–37 (1999).
- Piotrowski, J. & Chollet, H. Wheel-rail contact models for vehicle system dynamics including multi-point contact. *Veh. Syst. Dyn.* **43**(6/7), 455–483 (2005).
- Ren, Z. & He, X. Study on the characteristics of wheel/Rail Force Transfer and distribution on turnout zone. *China Railw. Sci.* **1**, 1–6 (2008).
- Yu, R. & Chen, J. A new method for wheel–rail contact force continuous measurement using instrumented wheelset. *Veh. Syst. Dyn.* **57**, 269–285 (2019).
- Nong, H. Study on methods for continuous measurement and identification of the vertical interaction between wheel/rail. PHD thesis. Southwest Jiaotong University (2007).
- Yang, Z., Gong, W. & Lu, Z. The elastic mechanics solution method of beam under several typical loads. *Mech. Eng.* **45**(1), 206–212 (2023).
- ANSYS. Release 16.0—Ansys Inc, Canonsburg Southpoint, PA 15317, USA (2016).

Author contributions

PingLu. and Xinyi Li. Ddabin Cui wrote the main manuscript text and built the models. Boyang An. Wenpeng Jiang. prepared figures and tables. All authors reviewed the manuscript.

Funding

This work was supported by supported by National Natural Science Foundation of China [grant number 52475137], Sichuan Science and Technology Program [grant number 2024YFHZ0280], Sichuan Nature and Science Foundation Innovation Research Group Project [grant number 2023NSFSC1975] and Foundation of Sichuan Provincial Engineering Research Center of Rail Transit Lines Smart Operation and Maintenance, Chengdu Vocational & Technical College of Industry, Vocational & Technical College of Industry [grant number 2024GD-Y10].

Competing interests

The authors declare no competing interests.

Additional information

Correspondence and requests for materials should be addressed to D.C.

Reprints and permissions information is available at www.nature.com/reprints.

Publisher's note Springer Nature remains neutral with regard to jurisdictional claims in published maps and institutional affiliations.

Open Access This article is licensed under a Creative Commons Attribution-NonCommercial-NoDerivatives 4.0 International License, which permits any non-commercial use, sharing, distribution and reproduction in any medium or format, as long as you give appropriate credit to the original author(s) and the source, provide a link to the Creative Commons licence, and indicate if you modified the licensed material. You do not have permission under this licence to share adapted material derived from this article or parts of it. The images or other third party material in this article are included in the article's Creative Commons licence, unless indicated otherwise in a credit line to the material. If material is not included in the article's Creative Commons licence and your intended use is not permitted by statutory regulation or exceeds the permitted use, you will need to obtain permission directly from the copyright holder. To view a copy of this licence, visit <http://creativecommons.org/licenses/by-nc-nd/4.0/>.

© The Author(s) 2025